

The distribution of $\text{ortho-H}_2\text{D}^+(1_{1,0}-1_{1,1})$ in L1544: tracing the deuteration factory in prestellar cores

C. Vastel¹

California Institute of Technology, Mail-code 320-47, Pasadena, CA 91125, USA

P. Caselli^{2,3}

*INAF - Osservatorio Astrofisico di Arcetri, Largo E. Fermi 5, 50125 Firenze, Italy
Harvard-Smithsonian Center for Astrophysics, 60 Garden St., Cambridge, MA 02138, USA*

C. Ceccarelli⁴

Laboratoire d'Astrophysique de l'Observatoire de Grenoble, BP 53, 38041 Grenoble Cedex 9, France

T. Phillips¹

M.C. Wiedner⁵

I. Physikalisches Institut, Universität zu Köln, Zülpicher Str. 77, 50937 Köln, Germany

R. Peng⁶

Caltech Submillimeter Observatory, Hilo, HI, USA

M. Houde⁷

*Department of Physics and Astronomy, University of Western Ontario, London, Ontario N6A 3K7,
Canada*

C. Dominik⁸

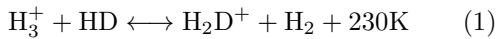
Sterrenkundig Instituut "Anton Pannekoek", Kruislaan 403, 1098 Amsterdam, The Netherlands

ABSTRACT

Prestellar cores are unique laboratories for studies of the chemical and physical conditions preceding star formation. We observed the prestellar core L1544 in the fundamental transition of $\text{ortho-H}_2\text{D}^+(1_{1,0}-1_{1,1})$ at different positions over $100''$, and found a strong correlation between its abundance and the CO depletion factor. We also present a tentative detection of the fundamental transition of $\text{para-D}_2\text{H}^+(1_{1,0}-1_{0,1})$ at the dust emission peak. Maps in N_2H^+ , N_2D^+ , HCO^+ and DCO^+ are used, and interpreted with the aid of a spherically symmetric chemical model that predicts the column densities and abundances of these species as a function of radius. The correlation between the observed deuterium fractionation of H_3^+ , N_2H^+ and HCO^+ and the observed integrated CO depletion factor across the core can be reproduced by this chemical model. In addition a simpler model is used to study the H_2D^+ ortho-to-para ratio. We conclude that, in order to reproduce the observed $\text{ortho-H}_2\text{D}^+$ observations, the grain radius should be larger than $0.3\ \mu\text{m}$.

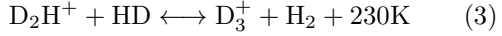
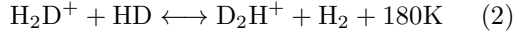
1. Introduction

Deuterium bearing species are good probes of the cold phases of molecular clouds prior to star formation. Many recent observations point to the fact that their abundances relative to their fully hydrogenated forms are larger, by factors up to 10^5 , than the solar neighborhood value of $\sim 1.5 \times 10^{-5}$ found by Linsky (2003). The deuterium fractionation has been evaluated in prestellar cores and low mass protostars from observations of HCO^+ and N_2H^+ (Butner et al. 1995; Williams et al. 1998; Caselli et al. 2002a; Crapsi et al. 2004, Crapsi et al. 2005), H_2CO (Loinard et al. 2001; Bacmann et al. 2003), H_2S (Vastel et al. 2003), HNC (Hirota et al. 2003), CH_3OH (Parise et al. 2004), and NH_3 (Roueff et al. 2000, Tiné et al. 2000). The chemical fractionation process in the gas-phase mainly arises from the difference between the zero-point energies of H_2 and HD . Almost incredibly, this can lead to a detectable quantity of triply deuterated molecules like ND_3 (Lis et al. 2002; van der Tak et al. 2002) and CD_3OH (Parise et al. 2004). The latter is thought to be formed mainly on dust grain surfaces (Charnley et al. 1997) in regions where the gas-phase $[\text{D}]/[\text{H}]$ ratio is enhanced to values larger than ~ 0.1 (Caselli et al. 2002c), as in the cold cores (see below). In molecular clouds, hydrogen and deuterium are predominantly in the form of H_2 and HD respectively. So the HD/H_2 ratio should closely equal the D/H ratio. Since the zero-point energies of HD and H_2 differ by ~ 410 K, the chemical fractionation will favor the production of HD compared to H_2 . In the dense, cold regions of the interstellar medium ($T \sim 10$ K), D will be initially nearly all absorbed into HD . The abundant ion available for interaction is H_3^+ , which gives H_2D^+ :



The reverse reaction does not occur efficiently in the cold dense clouds where low-mass stars form, and where the kinetic temperature is always below 25 K, the “critical” temperature above which reaction (1) starts to proceed from right to left and limits the deuteration. Therefore, the degree of fractionation of H_2D^+ becomes non-negligible. This primary fractionation can then give rise to other fractionations and form D_2H^+ and D_3^+ as

first suggested by Phillips & Vastel (2003):



We present in Figure 1 the main reactions involving these molecules. Note that the effect of the recombination of H_3^+ with electrons in the gas is negligible because of the low electron density in such regions. However, the effect of recombination with electrons on negatively charged grain surfaces becomes important when depletion increases (cf. Walmsley et al. 2004). The dissociation of the deuterated forms of H_3^+ is then responsible for the enhancement in the $[\text{D}]/[\text{H}]$ ratio. One specific parameter can enhance this process: the depletion of neutral species (in particular, the abundant CO) from the gas-phase (cf. Dalgarno & Lepp 1984). In fact, the removal of species which would normally destroy H_3^+ (e.g. CO; Roberts & Millar 2000) means that H_3^+ is more likely to react with HD and produce H_2D^+ , D_2H^+ and D_3^+ . The first model including D_2H^+ and D_3^+ (Roberts, Herbst & Millar 2003) predicted that these molecules should be as abundant as H_2D^+ (see also Flower et al. 2004).

Gas phase species are expected to be depleted at the center of cold, dark clouds, since they tend to stick onto the dust grains. A series of recent observations has shown that, in some cases, the abundance of molecules like CO decreases toward the core center of cold (≤ 10 K), dense (\geq a few 10^4 cm^{-3}) clouds. L1498: Willacy et al. (1998), Tafalla et al. (2002, 2004); IC 5146: Kramer et al. (1999), Bergin et al. (2001); L977: Alves et al. (1999); L1544: Caselli et al. (1999), Tafalla et al. (2002); L1689B: Jessop & Ward-Thompson (2001); Bacmann et al. (2002); Redman et al. (2002); B68: Bergin et al. (2002); L1517B: Tafalla et al. (2002, 2004); L1512: Lee et al. (2003); Oph D: Bacmann et al. (2003), Crapsi et al. (2005); L1521F: Crapsi et al. (2004); L183 (L134N): Paganini et al. (2005). These decreases in abundance have been interpreted as resulting from the depletion of molecules onto dust grains (see, e.g., Bergin & Langer 1997; Charnley 1997). It is now clear that these drops in abundance are typical of the majority of dense cores (see Tafalla & Santiago 2004 for the case of L1521E, the first starless core to be found with no molecular depletion).

In one of the most heavily CO depleted prestellar cores, L1544, Caselli et al. (2003) detected a strong (brightness temperature ~ 1 K) ortho- H_2D^+ (1₀₁-1₁₁) line, and concluded that H_2D^+ is one of the main molecular ions in the central region of this core. Encouraged by laboratory measurements (Hirao & Amano 2003), Vastel et al. (2004) detected the para- D_2H^+ molecule in its ground transition at 692 GHz. They found that, in the prestellar core 16293E, D_2H^+ is as abundant as H_2D^+ . These studies supported chemical modelling and the inclusion of multiply deuterated species (Roberts et al. 2003; Walmsley et al. 2004; Roberts et al. 2004; Flower et al. 2005; Aikawa et al. 2005). It appears that in dark clouds affected by molecular depletion, the deuterated forms of the molecular ion H_3^+ are unique tracers of the core nucleus, the future stellar cradle. Thus, their study becomes fundamental to the unveiling of the initial conditions of the process of star formation (kinematics, physical and chemical structure of pre-stellar cores).

In this paper, we present new observations of the H_2D^+ (1₁₀-1₁₁) line toward L1544, mapped over $\sim 100''$ of the dust peak emission, as well as a tentative detection of the D_2H^+ (1₁₀-1₀₁) line. Caselli et al. (2003) roughly estimated the size of the H_2D^+ emitting region in this pre-stellar core and suggested a radius of about 3000 AU. But this was based on a five-point map and cannot put stringent constraints on the chemical structure. Also a parallel study has been done by van der Tak et al. (2005) with the analysis of the line shape profile. Here, the H_2D^+ map is also compared with other high density tracer maps. Due to the poor atmospheric transmission at the frequency of the para- D_2H^+ fundamental line, this study is limited to the ortho- H_2D^+ fundamental line. We will present, in the last section, the perspectives on this work that will be opened up by future observatories.

2. Observations

The observations were carried out at the Caltech Submillimeter Observatory (CSO), between November 2003 and February 2005, under good weather conditions (225 GHz zenith opacity always less than 0.06) where the atmospheric transmission is about 30% at 372 GHz and less

than 20% at 692 GHz. Scans were taken toward the peak of the 1.3 mm continuum dust emission of L1544 ($\alpha_{2000} = 05^h 04^m 17^s.21$, $\delta_{2000} = +25^\circ 10' 42.8''$) using the chopping secondary with a throw of 3'. The 345 GHz (respectively 650 GHz) sidecab receiver with a 50 MHz acousto-optical spectrometer backend was used for all observations with a velocity resolution of 0.06 km s^{-1} (respectively 0.03 km s^{-1}) i.e. ~ 1.6 channels. At the observed frequencies of 372.421385(10) GHz for the H_2D^+ (1₁₀-1₁₁) and 691.660483(20) for the D_2H^+ (1₁₀-1₀₁) lines (Amano & Hirao 2005), the CSO 10.4 meters antenna has a HPBW of about $20''$ and $11''$ respectively. We mapped the area in H_2D^+ around the dust peak position with a grid spacing of $20''$ and used the value at the peak from Caselli et al. (2003) and integrated longer. The beam efficiency at 372 GHz (respectively 692 GHz) was measured on Venus, Saturn and Jupiter and found to be $\sim 60\%$ (respectively $\sim 40\%$). Pointing was monitored every 1 hour and half and found to be better than $3''$. In the case of H_2D^+ , the emission is extended compared to the beam size of CSO: the efficiency is then about 70%. If the emission in D_2H^+ is extended compared to the beamsize of $11''$, then the efficiency at 692 GHz is about 60%. The data reduction was performed using the CLASS program of the GAG software developed at IRAM and the Observatoire de Grenoble.

Figure 2 shows the H_2D^+ and D_2H^+ spectra observed toward the dust peak position. A Gaussian fit to the H_2D^+ line gives a LSR velocity of $\sim 7.3 \text{ km s}^{-1}$, but two peaks are clearly visible, with velocities 7.1 and 7.4 km s^{-1} (van der Tak et al. 2005), as also seen in other tracers (Tafalla et al. 1998; Caselli et al. 2002a). This central position has been originally observed by Caselli et al. (2003) and studied in detail by van der Tak et al. (2005); here, we improved the sensitivity and used the new value of the ortho- H_2D^+ (1₁₀-1₁₁) line frequency, recently measured by Amano & Hirao (2005). The on-source integration time for D_2H^+ is about 230 min. The D_2H^+ feature can be fitted with a gaussian with $T_a^* = 0.30 \pm 0.07 \text{ K}$, $\Delta v = 0.08 \pm 0.04 \text{ km s}^{-1}$ and $V_{LSR} = 7.29 \pm 0.03 \text{ km s}^{-1}$. The solid vertical line corresponds to the velocity from this gaussian fit. It is consistent with the central velocity of the H_2D^+ line of 7.28

$\pm 0.06 \text{ km s}^{-1}$. However, it is difficult to believe that the observed linewidth represents the real linewidth of the transition as the expected thermal linewidth is about 0.25 km s^{-1} for a kinetic temperature of 7 K, as predicted by dust temperature measurement (Evans et al. 2001; Zucconi et al. 2001). This is about 3 times larger than the observed linewidth. Formaldehyde observations of Bacmann et al. (2002) suggest larger gas temperatures (up to 9 K), but H₂CO is likely frozen in the core center, so that the measured temperature probably reflects the warmer core envelope (Young et al. 2004). At high densities (higher than $\sim 3 \text{ } 10^4 \text{ cm}^{-3}$), Young et al. (2004) find the gas and dust temperature to be between ~ 7 and 9 K, consistent with what was found by Tafalla et al. (2002) using ammonia. We will use in the following a temperature of 8 K in this cloud. The signal to noise ratio of our D₂H⁺ observations is not sufficient to get constraints on the kinematics of the source and the fitted linewidth probably does not represent the real linewidth. In absence of a possible explanation for the narrow linewidth for the D₂H⁺ profile, we will consider, in the following, that we only have a tentative detection, and will then use an upper limit.

Figure 3 shows the H₂D⁺ spectra around the central position (0'',0'') of the dust peak emission. The offset positions shown in the upper left are in arcseconds. A Gaussian fit for each detected line is plotted, using the CLASS program, and the line parameters are presented in Table 1. A double-peak profile seems to appear in the south-east as well as in the central part of the map. Considering the rms value, it is only possible to say that this non Gaussian profile is localized in the central positions around the dust peak emission. A possible interpretation could be the presence of two different layers with different velocities along the line of sight. Another explanation could be that the observed profiles are affected by absorption in a low-density (10^4 cm^{-3}) foreground layer redshifted ($\sim 0.08 \text{ km s}^{-1}$) relative to the high-density core, as found by (Williams et al. 1999) in the case of N₂H⁺(1-0) mapped at high spatial resolution. A more detailed study of the H₂D⁺ line profile toward the L1544 dust peak has been recently carried out by van der Tak et al. (2005), who suggested that the observed H₂D⁺ line, besides being broadened by the central infall, can

also be absorbed in the outer parts of the core. The presence of a central dip in the H₂D⁺ profile of at least four spectra across the L1544 map (see Fig. 3) favours this scenario.

Figure 4 shows the integrated intensity map ($\int T_{mbdv}$) of ortho-H₂D⁺ (1₁₀-1₁₁), together with maps of N₂H⁺ (1-0) and N₂D⁺ (2-1) obtained by Caselli et al. (2002a) and the 1.3 mm continuum emission map from Ward-Thompson et al. (1999), smoothed to a resolution of 22''. We note the close similarity between the H₂D⁺ and the N₂D⁺ maps and this will be discussed in the next sections. In this paper, we studied the chemistry using the maps made by Caselli et al. (2002a) in H¹³CO⁺, HC¹⁸O⁺, DCO⁺, D¹³CO⁺, C¹⁷O and C¹⁸O with the IRAM 30 m telescope.

3. Column density and abundance determinations

The observed molecular ions maps presented in Figure 4 show a general correlation, despite different beamwidths, with the distribution of dust continuum emission, in contrast to C¹⁸O (1-0) and C¹⁷O (1-0) (Caselli et al. 1999), which give clear evidence for depletion of CO at positions close to the continuum peak. H₂D⁺ (1₁₀-1₁₁), N₂D⁺ (2-1) and to a lesser spatial extent N₂H⁺ (1-0) appear to trace the dust continuum. From these maps N₂H⁺ does not seem to be depleted at the dust peak position.

In order to compare the observed species and put constraints on chemical models, we need to infer the column densities and abundances of H₂D⁺ and D₂H⁺ (defined as $N(i)/N(\text{H}_2)$ for a generic species *i*, with $N(\text{H}_2)$ derived from the 1.3 mm dust continuum emission map of Ward-Thompson et al. 1999). Assuming LTE conditions, we can estimate the optical depth at the line center from the observed line intensities:

$$T_{\text{mb}} = [J_{\nu}(T_{\text{ex}}) - J_{\nu}(T_{\text{bg}})](1 - e^{-\tau}) \quad (4)$$

where $J_{\nu}(T) = (h\nu/k)/(e^{h\nu/kT} - 1)$ is the radiation temperature of a blackbody at a temperature T, and T_{bg} is the cosmic background temperature of 2.7 K. The column density is then given by:

$$N_{\text{tot}} = \frac{8\pi\nu^3}{c^3} \frac{Q(T_{\text{ex}})}{g_u A_{\text{ul}}} \frac{e^{E_u/T_{\text{ex}}}}{e^{h\nu/kT_{\text{ex}}} - 1} \int \tau \, dv \quad (5)$$

where $Q(T_{ex})$ is the partition function:

$$Q(T_{ex}) = \sum_{i=0}^{\infty} (2I + 1) \exp(-E_i/kT_{ex}) \quad (6)$$

In the case of the H_2D^+ transition, $g_u = 9$, $A_{ul} = 1.04 \times 10^{-4} \text{ s}^{-1}$, $E_{ul} = 17.9 \text{ K}$; in the case of the D_2H^+ transition, $g_u = 9$, $A_{ul} = 4.55 \times 10^{-4} \text{ s}^{-1}$, $E_{ul} = 33.2 \text{ K}$. Using equation 4, we can estimate the upper limit on the D_2H^+ main beam temperature, under the assumption that the conditions of LTE are valid. With an excitation temperature of 8 K, the maximum main beam temperature reaches 0.53 K, which is about the observed main beam temperature of the D_2H^+ tentative detection, in the case where the spatial extent is larger than the beamsize of $11''$. The derived column densities depend on the assumed value of the excitation temperature. Within the 7–9 K temperature range, the column density at the dust peak can vary by a factor of 2. At larger distance, considering the increasing kinetic temperature and the decreasing molecular hydrogen density, the excitation temperature could be as low as 6 K. However, at these positions, the H_2D^+ column densities should only be decreased by a factor ~ 2.5 . Consequently we used a constant T_{ex} for our observations as an approximation. The corresponding line parameters and column densities are presented in Table 1. The upper limit on the para- D_2H^+ column density has been calculated using the thermal linewidth at 8 K (0.27 km s^{-1}).

At the $(0'', 0'')$ position, the column densities of ortho- H_2D^+ and para- D_2H^+ are $1.8 \times 10^{13} \text{ cm}^{-2}$ and $< 2.3 \times 10^{13} \text{ cm}^{-2}$, respectively (see Table 1). The abundances of species i , $X(i)$, have been determined dividing the column densities $N(i)$ by the associated H_2 column density derived from the 1.3 mm dust continuum emission. At the dust peak, we obtain $X(\text{ortho} - H_2D^+) \simeq 1.5 \times 10^{-10}$ and $X(\text{para} - D_2H^+) < 1.8 \times 10^{-10}$.

We present in Figure 6 the variation of the observed ortho- H_2D^+ , CO, H_2 , HCO^+ , DCO^+ , N_2H^+ , and N_2D^+ column densities (crosses) across the core (as a function of the impact parameter, the projected distance from the dust peak) as well as an upper limit on the para- D_2H^+ . Note that we used the ortho- H_2D^+ observations. We did not use any ortho-to-para ratio to estimate the total H_2D^+ column density or abundance because of the large uncertainty on this ratio. A

more thorough discussion on the ortho-to-para ratio for H_2D^+ and D_2H^+ will be performed in section 4.2.2. The observed column densities have then been averaged within the ranges delimited by the vertical dashed lines, at the positions $(2i + 1) \times 10''$ where $i=0,1,2,3\dots$ and are represented by triangles. The same computation was performed to present in Figure 7 the variation of the abundances as a function of the distance to the core center, limited to the central $70''$ ($r \sim 9800 \text{ AU}$). We will compare in section 4.1 these observations with the result from a best-fit model (dashed lines).

From Figures 6 and 7, we see that only CO is strongly depleted in the core center. Note that we used, in the CO column density computation: $^{16}\text{O}/^{18}\text{O}=560$ (Wilson & Rood 1994), and $^{18}\text{O}/^{17}\text{O}=4$ (Wouterloot et al. 2005; Ladd 2004). Defining the CO depletion factor, f_D , as the ratio of the CO “canonical” abundance ($[\text{CO}]/[\text{H}_2] = 9.5 \times 10^{-5}$; Frerking, Langer & Wilson 1982) and the observed CO abundance ($N(\text{CO})/N(\text{H}_2)$), Caselli et al. (1999) found $f_D = 10$ toward the dust peak and concluded that the most likely explanation for the low CO abundance is the freeze-out of CO onto dust grains at high densities ($n > 10^5 \text{ cm}^{-3}$). The corresponding radius of the depleted region is $r \sim 6500 \text{ AU} (\sim 45'')$.

The CO abundance is a critical parameter in the deuteration of the molecular ion H_3^+ (see Figure 1). In fact, from the abundance profiles presented in Figure 7 it is clear that the degree of deuterium enhancement (with DCO^+ , N_2D^+ , and H_2D^+) increases toward the dust peak emission of L1544 where CO is highly depleted, as previously found by Caselli et al. (2002b). N_2H^+ does not show any signs of depletion. It is mainly formed by interaction between H_3^+ and molecular nitrogen, which is likely to be the main repository of nitrogen in the gas phase. N_2 is only slightly less volatile than CO (factor of ~ 0.9 ; Öberg et al. 2005), so that the two neutrals are expected to behave similarly. However, N_2H^+ is destroyed by CO (Bergin et al. 2001, 2002; Pagani et al. 2005; Aikawa et al. 2005), so that the CO freeze-out implies a drop in the destruction rate of N_2H^+ , which at least partially balance the lower formation rate due to the N_2 freeze-out (see also Aikawa et al. 2001 for a discussion on this point). In fact, N_2H^+

is observed to survive in the gas phase at higher densities ($\sim 10^6 \text{ cm}^{-3}$) compared to CO ($\sim 10^5 \text{ cm}^{-3}$). This is also confirmed by the deuterium fractionation observed in N_2H^+ (~ 0.2), about 5 times larger than that measured in HCO^+ (Caselli et al. 2002b). HCO^+ is mainly formed via $\text{H}_3^+ + \text{CO}$ and destroyed by dissociative recombination, so that its abundance is simply reduced by the freeze-out of CO, its parent species. From Figure 7 it seems that the HCO^+ abundance is reduced at the dust peak, and increases at larger distance.

3.1. Correlations

In Figure 8, we show the correlation between the ortho- H_2D^+ abundances at the $0''$, $\pm 20''$ and $\pm 40''$ distance from the dust peak and the CO depletion factor, the $\text{DCO}^+/\text{HCO}^+$ ratio and the $\text{N}_2\text{D}^+/\text{N}_2\text{H}^+$ ratio. As intuitively expected, the ortho- H_2D^+ abundance appears to be well correlated with the CO depletion factor (see Figure 1). Also, the degree of deuterium enhancement in the HCO^+ and N_2H^+ molecules (measured from the $\text{DCO}^+/\text{HCO}^+$ and $\text{N}_2\text{D}^+/\text{N}_2\text{H}^+$ ratios) increases linearly with the ortho- H_2D^+ abundance. The χ^2 parameter is calculated for the three points where the impact parameters are $0''$, $20''$ and $40''$:

$$\chi^2 = \sum_{i=0}^2 \left(\frac{X_{\text{obs}}(i) - X_{\text{fit}}}{\sigma_{X_{\text{obs}}(i)}} \right)^2 \quad (7)$$

where X_{obs} and X_{fit} are the observed and fit values of the abundance respectively, and $\sigma_{X_{\text{obs}}}$ is the uncertainty in X_{obs} . The associated probabilities are reported when a correlation is established. The surprisingly high confidence level for the correlations between H_2D^+ and the degree of deuteration in the HCO^+ and N_2H^+ molecules ($\sim 100\%$), confirms that H_2D^+ dominates the fractionation of these molecules at low temperatures.

4. Chemical modelling

In this section we will interpret the observations using chemical models. We will adopt a two-way strategy. First (in section 4.1), we use a full chemical model applied to a density structure derived from continuum observations to produce an overall fit to all line observations presented in the previous section. In a second step (section 4.2), we

use a simplified chemical model focussing on the chemistry of H_3^+ deuteration, in order to better understand the relation between CO depletion and deuteration, and even to provide some estimates of the ortho-to-para ratio in the deuterated forms of H_3^+ that can be derived from our observations.

4.1. The “best-fit” model

To more quantitatively understand the column density and abundance correlations shown in Figures 6, 7 we used the model described in Caselli et al. (2002b), updated so that it now includes the multiply deuterated forms of H_3^+ (as in Crapsi et al. 2005) and new values of the binding energies of CO and N₂, following the measurements by Öberg et al. (2005) as well as other modifications to better account for the physical structure of the core. Briefly, the model considers a spherically symmetric cloud, with the density gradient as derived by Tafalla et al. (2002), using the 1.3 mm dust continuum emission data from Ward-Thompson et al. (1999), where the central density is $n(\text{H}_2) = 1.4 \times 10^6 \text{ cm}^{-3}$ (see Figure 5). The temperature profile has been included, using the recent findings of Young et al. (2004), where the temperature is about 7.5 K at the center and reaches about 12 K at the edge (see Figure 5). The chemical network contains CO, O and N₂, which can freeze-out onto dust grains and desorb due to cosmic-ray impulsive heating (as in Hasegawa and Herbst 1993). The initial abundances are: $X_i(\text{CO}) = 9.5 \times 10^{-5}$ (cf. Frerking et al. 1982), $X_i(\text{N}_2) = 4.0 \times 10^{-5}$ (slightly smaller than 6.6×10^{-5} , the cosmic value from Snow & Witt 1996, assuming that all nitrogen is in molecular form), and $X_i(\text{O}) = X_i(\text{CO})/2$, a factor of two less than what is typically found in gas-phase-only chemical models (e.g. Lee et al. 1996). The abundances of the molecular ions (N_2H^+ , H_3O^+ and HCO^+ and their deuterated forms) are calculated in terms of the instantaneous abundances of neutral species, assuming that the timescale for ion chemistry is much shorter than that for freeze-out. The electron fraction has been computed, as described in Caselli et al. (2002b), using a simplified version of the reaction scheme of Umebayashi & Nakano (1990), where the chemistry of a generic molecular ion “mH⁺” is taken into account, assuming formation due to proton transfer with H and destruction by dissociative recombi-

nation with electrons and recombination on grain surfaces (using rates from Draine & Sutin 1987). The “MRN” grain size distribution has been used (Mathis, Rumpl & Nordsieck 1977). We adopted the rate coefficients for the proton–deuteron exchange reactions recently measured by Gerlich et al. (2002). The model is run until the column density of C^{17}O toward the core center reaches the observed value ($N(\text{C}^{17}\text{O}) = 6 \times 10^{14} \text{ cm}^{-2}$; Caselli et al. 2002b).

The “best-fit” parameters of the model, which best reproduce the observed molecular column densities at the dust peak and the observed column density and abundance profiles, are the following:

- a cosmic-ray ionization rate of $\zeta = 1.3 \times 10^{-17} \text{ s}^{-1}$, standard value, typically used in chemical models (since Herbst & Klemperer 1973),
- binding energies for CO and N_2 of $E_{\text{D}}(\text{CO}) = 1100 \text{ K}$ and $E_{\text{D}}(\text{N}_2) = 900 \text{ K}$, values close to the binding energies measured for CO on water ice (Collings et al. 2003); the ratio between N_2 and CO binding energies (0.8) being comparable to the value (0.9) recommended by Öberg et al. (2005),
- a binding energy for atomic oxygen of $E_{\text{D}}(\text{O}) = 750 \text{ K}$, used in current gas–grain chemical models (e.g. Aikawa et al. 2005),
- a minimum size of the dust grains, in the MRN distribution of $a_{\text{min}} = 5 \times 10^{-6} \text{ cm}$ (10 times larger than in MRN),
- a sticking coefficient of $S = 1.0$ (Burke & Hollenbach 1983),
- an initial abundance of metals (assumed to freeze-out with a rate similar to that of CO), $X(\text{M}^+) = 10^{-6}$.

In Figures 6, 7, 8 we overlaid the results from the best-fit model (in dashed lines), to the observations. For the H_2D^+ plots, we present the ortho- H_2D^+ observation points, and scaled the total- H_2D^+ result from the model by 2.3, the factor between the predicted and the observed value at the dust peak position (assumed constant across the core). From this, an ortho-to-para ratio of ~ 0.8 can be deduced for H_2D^+ , but, considering the

uncertainties associated with this parameter (e.g. Pagani et al. 1992, Flower et al. 2005), we will postpone a discussion on this topic in the following section, where a parameter space exploration will be presented. For the D_2H^+ plot, we present the upper limit on the observed para- D_2H^+ compared with the (total) D_2H^+ result from the model. The ortho- H_2D^+ column densities and abundances observed at $0''$, $\pm 20''$ and $\pm 40''$ are well reproduced by the model, within the error bars (see Figures 6, 7). Note that although we need to assume a high degree of CO depletion in order to explain the CO observations, it appears that the HCO^+ column density is slightly under-estimated for the model at the dust peak emission. However, the strong variation (factor of 2) seen in Figure 6 between $0''$ and $15''$ could decrease the central HCO^+ column density. The discrepancy between the HCO^+ and DCO^+ column densities at larger distances can be explained by the uncertainties on the optical depth, since the less optically thick isotopes (HC^{18}O^+ and D^{13}CO^+) have only been used for the central position. Also the beamsize for the HC^{18}O^+ observations is larger (by 50%) than the $20''$ range.

Some N_2 depletion is needed in order to explain the N_2H^+ and N_2D^+ observations. Through the hyperfine structure of these species we can determine directly the optical depth in several transitions using the relative intensities of the hyperfine satellites. This considerably reduces the error in our computations, compared to other species like HCO^+ and DCO^+ .

This detailed model of the ion chemistry in L1544 simulates the observed depletion in the core center, and can reproduce the observed dependency of the column densities and abundances of species such as N_2H^+ , N_2D^+ , HCO^+ , DCO^+ as a function of the impact parameter. This allows us to separately discuss the relative contributions from the high-density depleted core and the lower density foreground (and background) gas.

4.2. Chemical parameter space exploration

In order to focus and analyse in detail the H_2D^+ chemistry, we performed a parameter study using a model that computes the deuterated forms of H_3^+ as a function of some key parameters, like

the grain size, the age of the L1544 condensation, and the cosmic rays ionization rate. This method has the advantage of concentrating on the H_2D^+ chemistry, avoiding to reproduce other molecular observations. Before discussing the comparison of the theoretical predictions with the observations, we give a short description of the model used.

It is an adaptation of the Ceccarelli & Dominik (2005) model, which has been developed for the proto-planetary disks. It computes the H_3^+ , H_2D^+ , D_2H^+ and D_3^+ abundances in cold and dense gas. Since the involved temperatures (≤ 30 K) and densities ($\geq 10^5 \text{ cm}^{-3}$) are very similar to those found around L1544, the model can be used directly, by just changing the geometry. For an easy and straightforward comparison with the observations we compute the H_3^+ chemistry in a gas cube with a given density and temperature. The relative abundances of the H_3^+ deuterated forms are computed solving the charge equilibrium equations and the deuterium chemistry equations.

In this model we also consider grains as a possible source of H_3^+ , H_2D^+ , D_2H^+ and D_3^+ destruction. In practice, the larger the CO depletion, the larger the $\text{H}_2\text{D}^+/\text{H}_3^+$ and $\text{D}_2\text{H}^+/\text{H}_2\text{D}^+$ ratios.

Two factors (other than the dust temperature) can modify the CO depletion : the age of the condensation (larger ages give larger CO depletions because the molecules have more time to freeze out onto the grains), and the gas density (the condensation rate is proportional to the gas density). In addition, the cosmic ray ionization rate regulates the overall ionization degree in the condensation, and therefore the H_3^+ isotopomers abundances. Finally, the grain sizes enter both in the CO condensation rate (via the grains area), and in the charge balance, because negatively charged grains recombine with the positively charged molecular ions. In this model, we adopted the same parameters (binding energy for CO and N_2 , sticking coefficient) chosen for our best-fit model (see section 4.1).

4.2.1. H_2D^+ and D_2H^+ versus CO depletion

In Figure 9, we present the results of the model, varying the three key parameters of the model (cosmic ionization rate, the grain radius and the age of the core) in order to reproduce the total (ortho + para) H_2D^+ and D_2H^+ abundances. We

plot the abundances as a function of depletion because this parameter is more directly observed (via CO column density and dust continuum observations) than the gas density. We also make a comparison with the observations of ortho- H_2D^+ and para- D_2H^+ to get an insight into the deuterium chemistry of H_3^+ .

We fixed the temperature of the cloud in the model to 8 K, which is within the range found from molecular and dust measurements. For comparison we also ran the cases with a temperature of 10 K and did not find any substantial difference. The free-fall time is approximately 3×10^4 years for a density of about 10^6 cm^{-3} . In presence of a magnetic field, the collapse time is about an order of magnitude larger (Ciolek & Basu 2000). We will vary the age between 10^4 to 10^6 years, the latter being close to the lifetime of a starless core. In our calculations, we assumed all the grains in the cloud to have the same size, but we investigated the result for different values of the grain radius. A grain size of $0.1 \mu\text{m}$ is the typical value assumed in chemical models for the interstellar medium, where it follows the MRN distribution. In the upper plot of Figure 9 we used a standard cosmic ionisation rate of $3 \times 10^{-17} \text{ s}^{-1}$, a typical age of 10^5 years and varied the dust grain averaged sizes between $0.05 \mu\text{m}$ and $0.2 \mu\text{m}$. In the middle plot we fixed the age to 10^5 years, the grain size to $0.1 \mu\text{m}$ and varied the cosmic ionization rate between 3×10^{-18} to $3 \times 10^{-16} \text{ s}^{-1}$. In the lower plot we fixed the grain size to $0.1 \mu\text{m}$, the cosmic ionization rate to $3 \times 10^{-17} \text{ s}^{-1}$ and varied the age of the cloud between 10^4 and 10^6 years. The observation points (or upper limit in the case of D_2H^+) and their corresponding error bars are superposed in these plots: ortho- H_2D^+ on the left side and para- D_2H^+ on the right side.

As the grain size increases while the total grain mass is conserved, the abundance of grains relative to H_2 decreases $\propto a_{\text{grain}}^{-3}$, and also the grain surface area per H_2 decreases $\propto a_{\text{grain}}^{-1}$. As this effect slows down the freezeout of CO, the same CO depletion is therefore reached either after a longer time, or at a higher density. Since we keep the age constant, the effect of the density is observed in Figure 9: larger grain sizes correspond to higher densities, at which the overall degree of ionization is smaller. Since H_2D^+ is the dominating ion, this is directly mirrored in the H_2D^+ abundance. Also, decreasing the cosmic ionization rate leads to a decrease

in the abundances. Indeed, H_3^+ ions (and consequently their deuterated forms) are formed by the ionization of H_2 due to cosmic rays. And finally, increasing the age of the cloud will increase their abundances, as the CO depletion rate is time dependant. Consequently, for a more evolved cloud the same CO depletion is achieved for lower densities, corresponding to a higher degree of ionization, which is again directly reflected in the H_2D^+ and D_2H^+ abundances.

4.2.2. The ortho and para forms

Both H_2D^+ and D_2H^+ molecules have ortho and para forms, corresponding to the spin states of the protons (for H_2D^+) or deuterons (for D_2H^+). In order to compare the modeled abundances with the observations of one spin state only, it is critical to know the ortho-to-para ratio for these two molecules. Under LTE conditions, at temperature T , the relative populations of the lowest ortho ($1_{1,1}$) and para ($0_{0,0}$) levels of H_2D^+ would be:

$$\frac{n(1_{1,1})}{n(0_{0,0})} = 9 \times \exp\left(-\frac{86.4}{T}\right) \quad (8)$$

and the relative populations of the lowest ortho ($0_{0,0}$) and para ($1_{0,1}$) levels of D_2H^+ would be:

$$\frac{n(1_{0,1})}{n(0_{0,0})} = \frac{9}{6} \times \exp\left(-\frac{50.2}{T}\right) \quad (9)$$

With these formulae, at 8 K, the H_2D^+ ortho-to-para ratio would be $\sim 1.8 \times 10^{-4}$ and the D_2H^+ para-to-ortho ratio would be $\sim 2.8 \times 10^{-3}$. The ortho form of H_2D^+ is produced mainly in reactions of the para form with ortho- H_2 (e.g. Gerlich, Herbst & Roueff 2002). Therefore, its high o/p ratio is attributable to the relatively high ortho- H_2 abundance as first noticed by Pagani et al. (1992). Because the o/p ratio is not thermalized at the low temperature considered here, the o/p H_2D^+ ratio is not thermalized either. This can be illustrated in Flower, Pineau des Forêts, Walmsley (2004) model where, at temperatures lower than 10 K, a hydrogen density of $2 \times 10^6 \text{ cm}^{-3}$ and a grain size of $0.1 \mu\text{m}$, the o/p- H_2D^+ reaches unity and the p/o- D_2H^+ value is about 0.1. Increasing the grain size will decrease the grain surface, leading to a decrease of the H_2 formation rate. Therefore, the H_2 ortho-to-para ratio will obviously decrease, as well as the H_2D^+ ortho-to-para ratio.

From our observations we find that para- D_2H^+ /ortho- H_2D^+ is less than 1.3 at the dust peak emission assumed to be at 8 K. In the prestellar core 16293E (Vastel et al. 2004) we measured a para- D_2H^+ /ortho- H_2D^+ of 0.75 for an excitation temperature of 10 K. We also computed the H_2D^+ ortho-to-para ratio and an upper limit on the D_2H^+ para-to-ortho ratio by comparing the observed abundances of ortho- H_2D^+ and para- D_2H^+ with the total (ortho + para) abundances of H_2D^+ as calculated using the model described in the previous section. In Table 2, the ortho-to-para ratio for H_2D^+ and the para-to-ortho ratio for D_2H^+ are quoted in order to reproduce the values obtained by the model for different sets of parameters, which are the cosmic ionization rate, the age of the core and the grain radius. We can directly compare our results on H_2D^+ with the Flower, Pineau des Forêts, Walmsley (2004) model, even if their study assumes complete depletion (i.e. that CO abundance should be less than 10^{-6}). Indeed the abundance of both ortho and para spin states of H_2D^+ depends on the ortho and para forms of molecular hydrogen (through the proton-exchanging reaction of H_3^+ with H_2 followed by reaction 1) which does not vary as a function of depletion. On the contrary, the abundance of both para and ortho forms of D_2H^+ is determined by reactions with HD (produced on the grain surfaces) and will therefore depend on the core depletion. The Flower et al. model predicts H_2D^+ ortho-to-para ratios larger than the maximum value of 0.3 we observed for a temperature of 8 K and a H_2 density of $2 \times 10^6 \text{ cm}^{-3}$ (Pineau des Forêts, *private communication*) spanning ranges up to $0.4 \mu\text{m}$ of the grain radius. As a consequence, since the H_2D^+ ortho-to-para ratio decreases as a function of the grain radius, it is likely that this should be larger than $0.3 \mu\text{m}$. This depletion of small grains in this core is consistent with grain coagulation since ice condensation is not enough to increase the grain radius.

5. Conclusions and Perspectives

In this paper we studied the prestellar core L1544, focusing on the H_2D^+ chemistry throughout the cloud. It is now widely accepted that the H_2D^+ molecule is the main tracer of the CO depleted prestellar cores, and we point out in this paper that the H_2D^+ emission is extended (over

60''), and an excellent tracer of the dust continuum, with a emitting radius of about 7,000 AU in the case of L1544. Hence, the line profile of this molecule would provide a crucial guide to the dynamical behavior of the high-density core. It is likely that the double-peak profile found in the central position, as well as positions around, is broadened by the central infall and is absorbed in the outer parts of the core (van der Tak et al. 2005).

We first used a model of the ion chemistry coupled with the physical structure of the core of L1544, including the deuterated isotopologues of the H_3^+ ion. This simulates the observed depletion and can approximatively reproduce the observed dependence of the column densities of species like N_2H^+ , N_2D^+ , HCO^+ , DCO^+ , H_2D^+ as a function of radius.

This study reveals a correlation between the ortho- H_2D^+ abundance and 1) the CO depletion factor, 2) the degree of deuteration in the HCO^+ molecule, 3) the degree of deuteration in the N_2H^+ molecule. H_2D^+ will survive longer, at higher density than N_2H^+ and N_2D^+ .

We then used a simpler model focusing on the H_2D^+ chemistry where we did a wide parameter study. We discuss how the H_2D^+ and D_2H^+ abundances depend on the cosmic ionization rate, the age of the core, and the grain radius, by varying these parameters. It appears that the most important parameters to reproduce the observed values is the grain radius as small grains accelerate the freeze-out of CO and the observed values are consistent with a freeze-out rate dominated by larger grains. Therefore, we found that to reproduce the observations we need a larger grain radius of 0.3 μm .

This study can be considered as a springboard for observations to come, since the current observations are limited by the poor atmospheric transmission at the relevant frequencies. Table 3 lists some of the major telescopes and interferometers that can be used for the study of H_2D^+ chemistry in prestellar cores, proto-planetary disks and protostars. Probably, D_3^+ can not be observable because enhanced D_3^+ abundance implies very cold and very dense regions. Since D_3^+ is a symmetric molecule, it does not have rotational transitions and does have its bending modes are in the near infrared. Therefore, these transitions will only

be observable in absorption against a strong near infrared continuum. H_2D^+ and D_2H^+ are hence the only tracers of cold, dense phases of molecular clouds prior to star formation.

The authors thank the staff of the CSO telescope for their support. CV is grateful to Malcom Walmsley for fruitful discussions and to Laurent Pagani for useful comments. PC acknowledges support from the MIUR grant "Dust particles as factor of galactic evolution". This research has been supported by NSF grant AST-0540882 to the CSO.

Facilities: CSO.

REFERENCES

Aikawa, Y., Ohashi, N., Inutsuka, S.-i., Herbst, E., & Takakuwa, S. 2001, ApJ, 552, 639

Aikawa, Y., Herbst, E., Roberts, H., & Caselli, P. 2005, ApJ, 620, 330

Alves, J., Lada, C.J. & Lada, E.A., 1999, ApJ, 515, 265

Amano, T., & Hirao, T., 2005, J. Mol. Spectroscopy, 233, 7

André, P., Ward-Thompson & D., Barsony, M., 2000, in Protostars and Planets IV, ed. M. M. Matthews, V., Boss, A.P., Russel, S.S.

Bacmann, A., Lefloch, B., Ceccarelli, C., Castets, A., Steinacker, J., & Loinard, L., 2002, A&A 389, 6

Bacmann, A., Lefloch, B., Ceccarelli, C., Steinacker, J., Castets, A., & Loinard, L. 2003, ApJ, 585, L55

Bergin, E.A. & Langer, W.D., 1997, ApJ 486, 316

Bergin, E., Ciardi, D., Lada, C.J., Alves, J., & Lada, E.A., 2001, ApJ 557, 209

Bergin, E. A., Alves, J., Huard, T., & Lada, C. J. 2002, ApJ, 570, L101

Burke, J. R., & Hollenbach, D. J. 1983, ApJ, 265, 223

Butner, H. M. and Lada, E. A. & Loren, R. B., 1995, ApJ, 448, 207

Caselli, P., Walmsley, C.M., Tafalla, M., Dore, L., & Myers, P.C., 1999, ApJ 523, L165

Caselli, P., Walmsley, C.M., Zucconi, A., Tafalla, M., Dore, L. & Myers, P.C., 2002, ApJ 565, 331

Caselli, P., Walmsley, C.M., Zucconi, A., Tafalla, M., Dore, L. & Myers, P.C., 2002, ApJ 565, 344

Caselli, P., Stantcheva, T., Shalabiea, O., Shemtovitch, V. & Herbst, E., 2002, P&SS 50, 1257

Caselli, P., van der Tak, F., Ceccarelli, C. & Bacmann, A., 2003, A&A 403, L37

Ceccarelli, C., & Dominik, C. 2005, A&A, 440, 583

Charnley, S.B., 1997, MNRAS 291, 455

Ciolek, G. E., & Basu, S. 2000, ApJ, 529, 925

Collings, M. P., Dever, J. W., Fraser, H. J., McCoustra, M. R. S., & Williams, D. A. 2003, ApJ, 583, 1058

Crapsi, A., Caselli, P., Walmsley, C. M., Tafalla, M., Lee, C. W., Bourke, T. L., & Myers, P. C. 2004, A&A, 420, 957

Crapsi, A., Caselli, P., Walmsley, C. M., Myers, P. C., Tafalla, M., Lee, C. W., & Bourke, T. L. 2005, ApJ, 619, 379

Dalgarno, A., & Lepp, S. 1984, ApJ, 287, L47

Draine, B. T., & Sutin, B. 1987, ApJ, 320, 803

Evans, N.J. II, Rawlings, J.M.C., Shirley, Y. & Mundy, L.G., 2001, ApJ 557, 193

Flower, D.R., Pineau des Forets, G. & Walmsley, C.M., 2004, A&A 427, 887

Flower, D. R., Pineau Des Forêts, G., & Walmsley, C. M. 2005, A&A, 436, 933

Frerking, M. A., Langer, W. D., & Wilson, R. W. 1982, ApJ, 262, 590

Gerlich, D., Herbst, E., & Roueff, E. 2002, Planet. Space Sci., 50, 1275

Hasegawa, T. I., & Herbst, E. 1993, MNRAS, 263, 589

Herbst, E., & Klemperer, W. 1973, ApJ, 185, 505

Hirao, T. & Amano, T., 2003, ApJ 597, L85

Hirota, T., Ikeda, M., & Yamamoto, S. 2003, ApJ, 594, 859

Jessop, N.E., Ward-Thompson, D., 2001, MNRAS 323, 1025

Kirk, J.M., Ward-Thompson, D., & André, P., 2005, accepted in MNRAS

Kramer, C., Alves, J., Lada, C.J., Lada, E.A., et al., 1999, A&A 342, 257

Ladd, E. F. 2004, ApJ, 610, 320

Lee, J.-E., Evans, N. J., Shirley, Y. L., & Tatematsu, K. 2003, ApJ, 583, 789

Linsky, J.L., 2003, Space Science Review 106, 49

Lis, D. C., Roueff, E., Gerin, M., Phillips, T. G., Coudert, L. H., van der Tak, F. F. S., & Schilke, P. 2002, ApJ, 571, L55

Loinard, L., Castets, A., Ceccarelli, C., Caux, E., & Tielens, A. G. G. M. 2001, ApJ, 552, L163

Mathis, J. S., Rumpl, W., & Nordsieck, K. H. 1977, ApJ, 217, 425

Öberg, K. I., van Broekhuizen, F., Fraser, H. J., Bisschop, S. E., van Dishoeck, E. F., & Schlemmer, S. 2005, ApJ, 621, L33

Pagani, L., Salez, M., & Wannier, P. G. 1992, A&A, 258, 479

Pagani, L., Pardo, J.-R., Apponi, A. J., Bacmann, A., & Cabrit, S. 2005, A&A, 429, 181

Parise, B., Castets, A., Herbst, E., Caux, E., Ceccarelli, C., Mukhopadhyay, I., & Tielens, A. G. G. M., 2004, A&A, 416, 159

Phillips, T.G. & Vastel, C., 2003, in "Chemistry as a diagnostic of star formation", ed. C. Curry & M. Fish, astro-ph/0211610

Redman, M. P., Rawlings, J. M. C., Nutter, D. J., Ward-Thompson, D., & Williams, D. A., 2002, MNRAS, 337, L17

Roberts, H. & Millar, T.J., 2000, A&A 361, 388

Roberts, H., Herbst, E. & Millar, T.J., 2003, ApJ 591, 41

Roberts, H., Herbst, E., & Millar, T. J. 2004, *A&A*, 424, 905

Roueff, E., Tiné, S., Coudert, L. H., Pineau des Forêts, G., Falgarone, E., & Gerin, M. 2000, *A&A*, 354, L63

Tafalla, M., Mardones, D., Myers, P. C., Caselli, P., Bachiller, R., & Benson, P. J. 1998, *ApJ*, 504, 900

Tafalla, M., Myers, P. C., Caselli, P., Walmsley, C. M., & Comito, C. 2002, *ApJ*, 569, 815

Tafalla, M., Myers, P. C., Caselli, P., & Walmsley, C. M. 2004, *A&A*, 416, 191

Tafalla, M., & Santiago, J. 2004, *A&A*, 414, L53

Tiné, S., Roueff, E., Falgarone, E., Gerin, M., & Pineau des Forêts, G. 2000, *A&A*, 356, 1039

Umebayashi, T., & Nakano, T. 1990, *MNRAS*, 243, 103

van der Tak, F. F. S., Schilke, P., Müller, H. S. P., Lis, D. C., Phillips, T. G., Gerin, M., & Roueff, E. 2002, *A&A*, 388, L53

van der Tak, F. F. S., Caselli, P., & Ceccarelli, C. 2005, *A&A*, 439, 195

Vastel, C., Phillips, T. G., Ceccarelli, C., & Pearson, J. 2003, *ApJ*, 593, L97

Vastel, C., Phillips, T. G., & Yoshida, H., *ApJL* 606, 127

Walmsley, C. M., Flower, D. R., & Pineau des Forêts, G. 2004, *A&A*, 418, 1035

Ward-Thompson, D., Motte, F., & André, P., 1999, *MNRAS* 305, 143

Willacy, K., Langer, W., & Velusamy, T., 1998, *ApJ* 507, 171

Williams, J. P., Bergin, E. A., Caselli, P., Myers, P. C., & Plume, R. 1998, *ApJ*, 503, 689

Williams, J., Myers, P., Wilner, D., & Di Francesco, J., 1999, *ApJ* 513, L61

Wilson, T. L., & Rood, R. 1994, *ARA&A*, 32, 191

Wouterloot, J. G. A., Brand, J., & Henkel, C. 2005, *A&A*, 430, 549

Young, K. E., Lee, J.-E., Evans, N. J., Goldsmith, P. F., & Doty, S. D. 2004, *ApJ*, 614, 252

Zucconi, A., Walmsley, C. M., & Galli, D. 2001, *A&A*, 376, 650

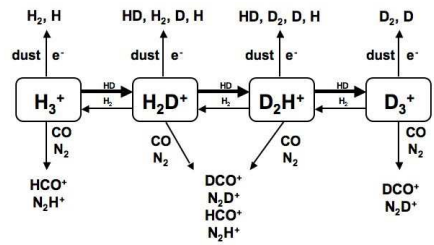


Fig. 1.— Main reactions involving the deuterated forms of the H_3^+ molecule. When CO and N_2 are depleted, the molecular reactions presented with bold arrows are dominant.

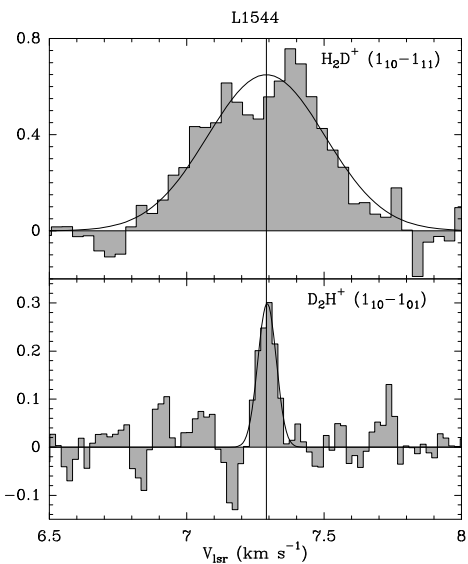


Fig. 2.— Ortho- H_2D^+ and para- D_2H^+ observations at the dust peak emission corresponding to the $(0'',0'')$ position. The temperatures are T_a^* in Kelvins. The vertical solid line corresponds to the velocity center of the D_2H^+ gaussian fit (7.29 km s^{-1}).

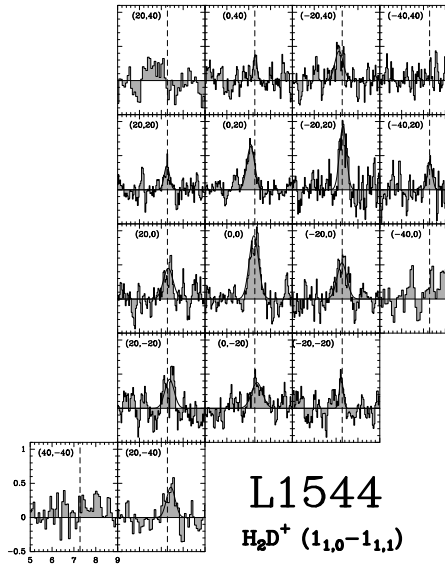


Fig. 3.— Map of the H_2D^+ ($1_{10}-1_{11}$) line centered on the dust peak of L1544. The Y-axis represents the main beam temperature. The position is indicated in arcseconds in right ascension and declination offsets from the central position, on the top left of each spectrum. The reference for the velocity center at the $(0'',0'')$ position (7.28 km s^{-1}) is indicated in dashed lines.

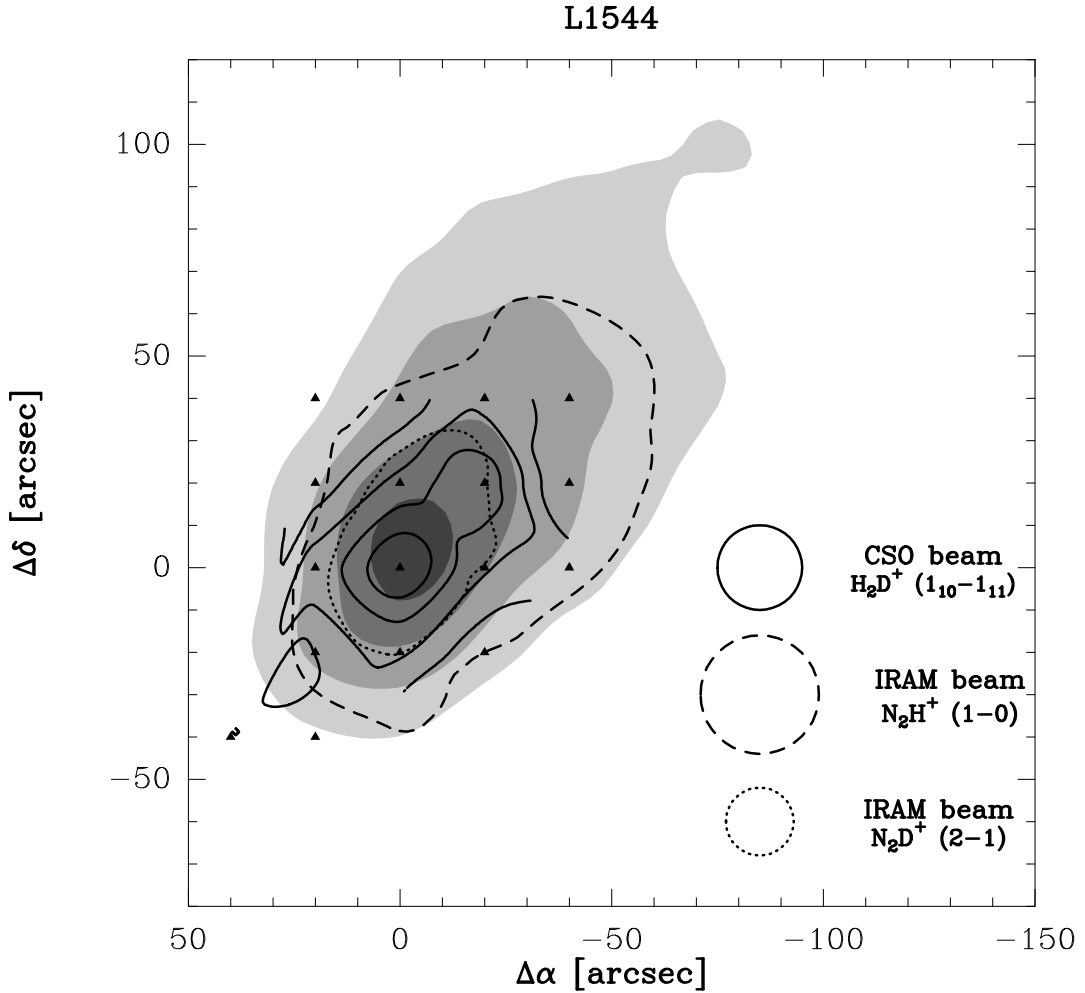


Fig. 4.— Integrated intensity maps of H_2D^+ ($1_{10}-1_{11}$), N_2H^+ (1-0) and N_2D^+ (2-1) superposed on the 1.3 mm continuum emission map smoothed to a resolution of $22''$ (gray scale). Contour levels are 30%, 50%, 70% and 90% of the peak (0.54 K km s^{-1} for H_2D^+), and 50% of the peak (5.5 K km s^{-1} for N_2H^+ and 2.1 K km s^{-1} for N_2D^+). The observed positions in H_2D^+ are reported as triangles. The $(0'',0'')$ position corresponds to $\alpha_{2000} = 05^h 04^m 17^s.21$, $\delta_{2000} = +25^\circ 10' 42.8''$. The beam sizes of the observations are also reported in the lower right corner of the figure.

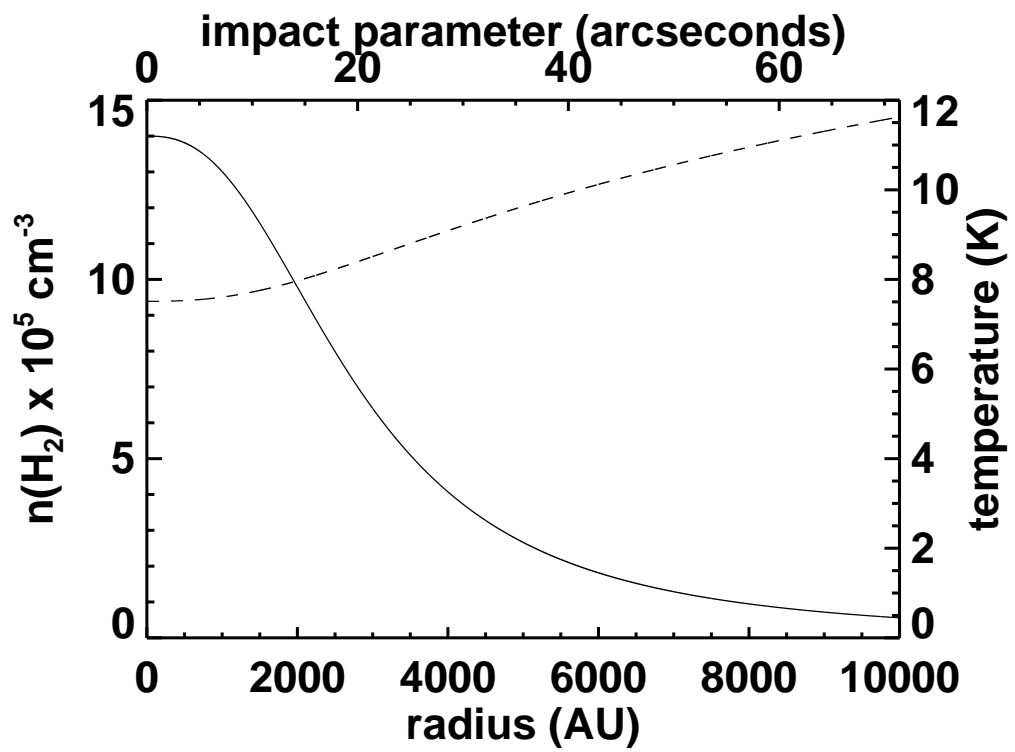


Fig. 5.— Density (plain line) and temperature (dashed line) profiles as a function of the radius (in astronomical units) or the impact parameter (in arcseconds), used for the best-fit model.

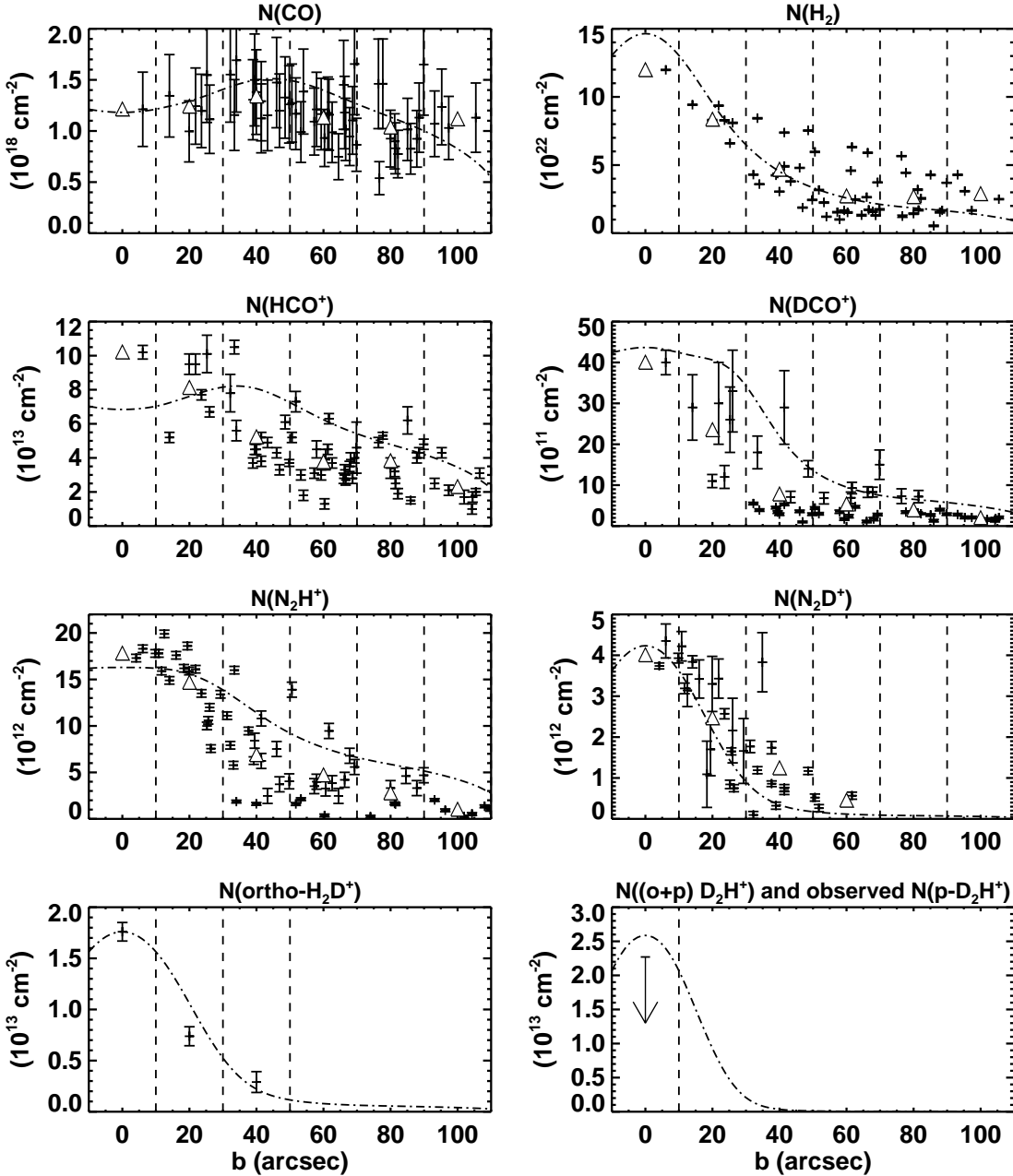


Fig. 6.— Variation of the CO (in a 20" beam), H₂, HCO⁺, DCO⁺, N₂H⁺, N₂D⁺, H₂D⁺ and D₂H⁺ column densities as a function of distance. The cross represent the observation points and the 3 σ error, the triangles represent the observation points averaged in the bins delimited by the dashed lines, and the dot-dashed lines represent the results from a "best-fit" model. For H₂D⁺, note that the variation of the observed ortho column density is compared with the modeled ortho variation (see text). Also for D₂H⁺, the upper limit on the para column density is reported on the plot of the modeled ortho + para variation.

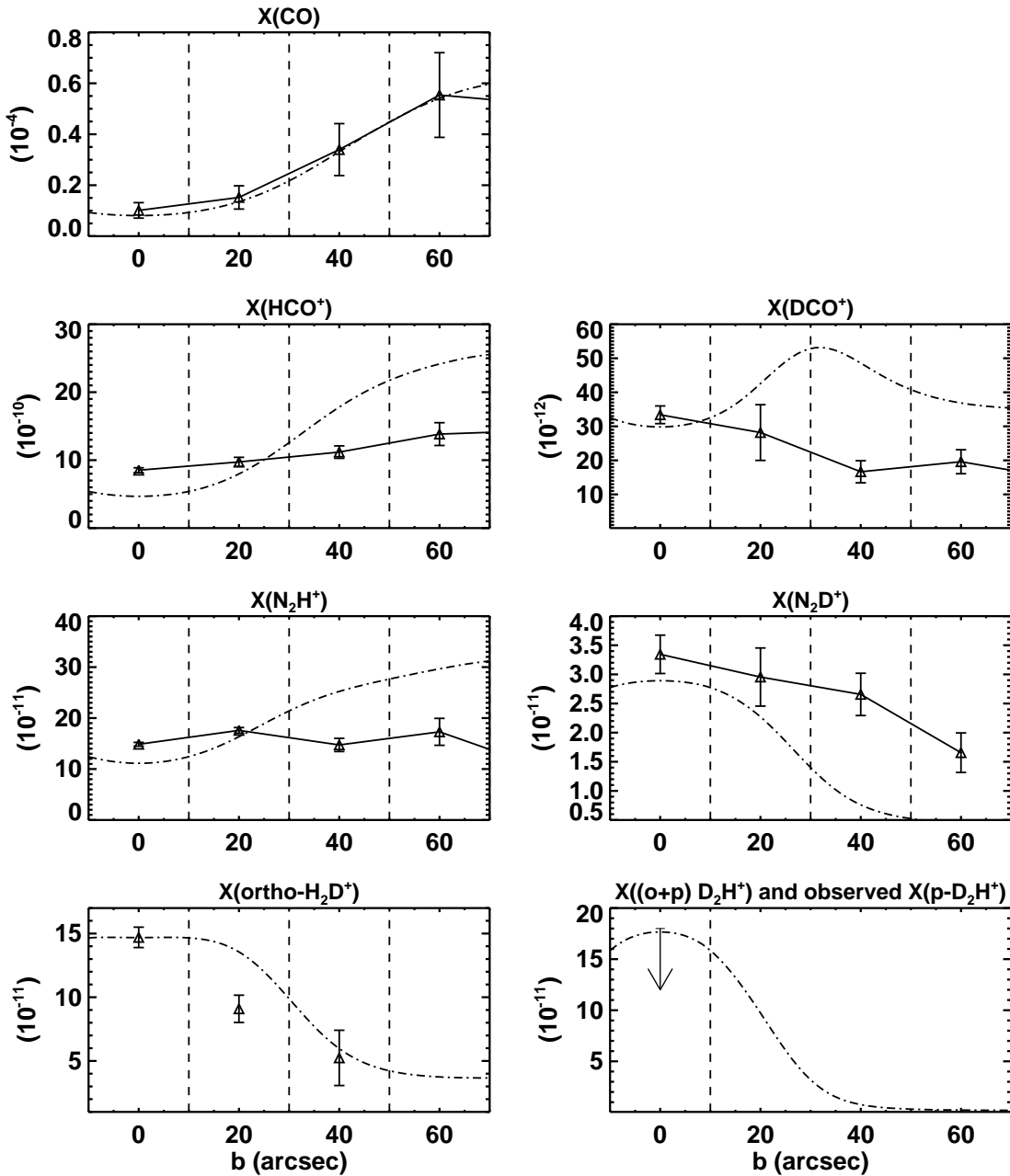


Fig. 7.— Variation of the CO (in a 20" beam), HCO⁺, DCO⁺, N₂H⁺, N₂D⁺, H₂D⁺ and D₂H⁺ abundances as a function of distance. The triangles represent the observation points averaged in the bins delimited by the dashed lines, and the dot-dashed lines represent the results from a "best-fit" model. For H₂D⁺, note that the variation of the observed ortho abundance is compared with the modeled ortho variation (see text). Also for D₂H⁺, the upper limit on the para abundance is reported on the plot of the modeled ortho + para variation.

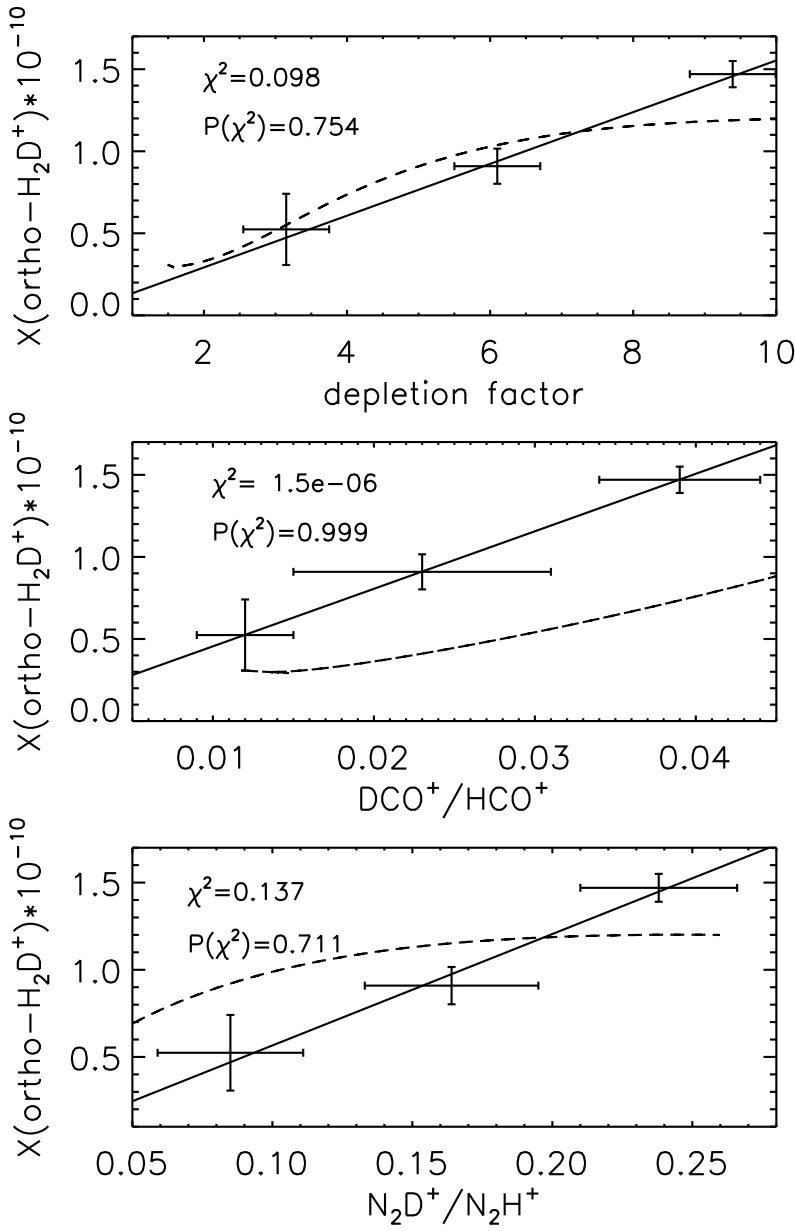


Fig. 8.— Variation of the observed ortho-H₂D⁺ as a function of the depletion factor, DCO⁺/HCO⁺ ratio and N₂D⁺/N₂H⁺ ratio. The χ^2 parameter and its probability are reported when a correlation is established. Superposed are the results from the best-fit model (see section 4.1)

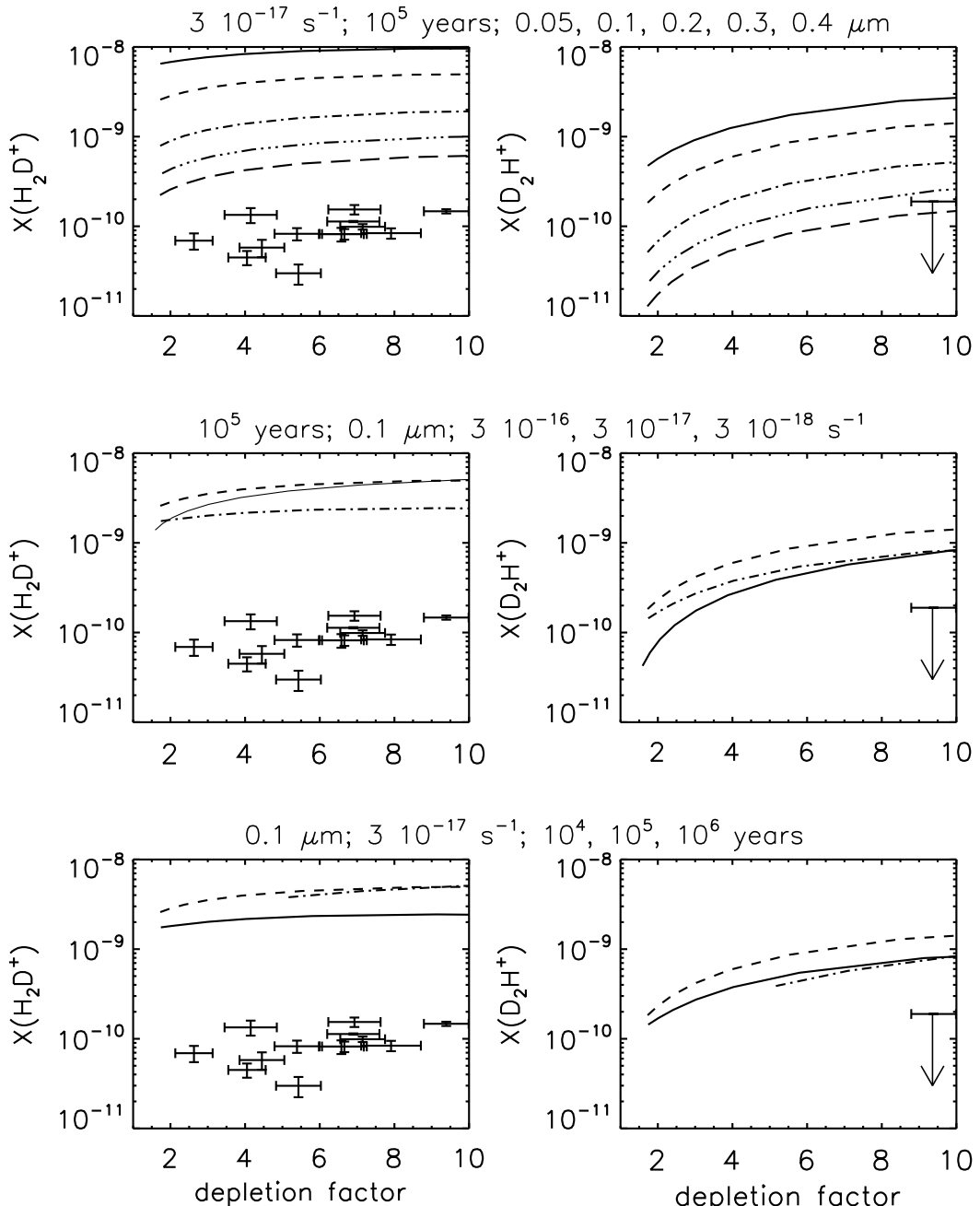


Fig. 9.— Variation of the H_2D^+ abundance (respectively D_2H^+) for the model (plain line) as a function of CO depletion factor. The points with the corresponding error bars represent the observed abundances of ortho- H_2D^+ and para- D_2H^+ towards L1544 whereas the lines show the modeled abundances of the ortho + para states. Hence we expect the observed values to lie below the modeled ones. The temperature was fixed to 8 K. In the upper plot we varied the grain size: 0.05, 0.1, 0.2, 0.3 and 0.4 μm . Note that increasing the grain size decreases the H_2D^+ and D_2H^+ abundances (see text). In the middle plot we varies the cosmic ionization ray: $3 \cdot 10^{-16}$ (plain line), $3 \cdot 10^{-17}$ (dashed line) and $3 \cdot 10^{-18} \text{ s}^{-1}$ (dot-dashed line).

Table 1: Lines parameters, and column densities of the ortho-H₂D⁺ and para-D₂H⁺ observations for an excitation temperature of 8 K. The 1 σ errors are noted in parenthesis. The upper limit (3 σ) on the para-D₂H⁺ column density has been determined using a linewidth of 0.27 km s⁻¹ (see section 3).

Position (")	rms (K)	V _{LSR} km s ⁻¹	Δv_{res} km s ⁻¹	Δv km s ⁻¹	$\int T_{mb} \Delta v$ mK km s ⁻¹	N(o-H ₂ D ⁺) cm ⁻²	tau
(0,0)	0.11	7.277(0.016)	0.039	0.50(0.03)	495(33)	1.78(0.10) 10 ¹³	0.58(0.05)
(20,0)	0.12	7.319(0.045)	0.039	0.52(0.12)	255(37)	7.77(1.01) 10 ¹²	0.24(0.04)
(0,-20)	0.10	7.382(0.040)	0.039	0.59(0.09)	232(33)	6.92(0.90) 10 ¹²	0.19(0.03)
(-20,0)	0.13	7.269(0.033)	0.039	0.52(0.06)	293(40)	9.14(1.10) 10 ¹²	0.29(0.05)
(-20,-20)	0.11	7.238(0.023)	0.039	0.20(0.06)	98(20)	2.99(0.58) 10 ¹²	0.24(0.05)
(-40,0)	0.13		0.077		< 49	< 1.46 10 ¹²	
(-40,20)	0.12	7.294(0.035)	0.039	0.27(0.07)	115(26)	3.45(0.73) 10 ¹²	0.21(0.05)
(-20,20)	0.21	7.316(0.018)	0.039	0.37(0.04)	386(54)	1.28(0.15) 10 ¹³	0.58(0.10)
(0,20)	0.08	7.094(0.015)	0.039	0.43(0.04)	288(22)	9.27(0.62) 10 ¹²	0.35(0.03)
(20,20)	0.09	7.256(0.026)	0.039	0.29(0.08)	111(15)	3.30(0.57) 10 ¹²	0.19(0.03)
(0,40)	0.11	7.300(0.024)	0.039	0.18(0.05)	75(20)	2.24(0.55) 10 ¹²	0.20(0.03)
(-20,40)	0.12	7.138(0.032)	0.039	0.45(0.09)	206(34)	6.24(0.94) 10 ¹²	0.23(0.04)
(-40,40)	0.10		0.039		< 27	< 4.52 10 ¹²	
(20,-20)	0.14	7.378(0.040)	0.039	0.49(0.06)	224(42)	6.79(1.15) 10 ¹²	0.23(0.04)
(20,40)	0.12		0.077		< 46	< 1.27 10 ¹²	
(20,-40)	0.11	7.436(0.054)	0.077	0.46(0.10)	215(45)	6.55(1.23) 10 ¹²	0.23(0.04)
(40,-40)	0.12		0.077		< 46	< 1.27 10 ¹²	

Position	rms	V _{LSR}	Δv_{res}	Δv	$\int T_{mb} \Delta v$	N(p-D ₂ H ⁺)	tau
(0,0)	0.072	7.290(0.007)	0.021	0.27	< 103	< 2.27 10 ¹³	< 1.13

TABLE 2

H_2D^+ ORTHO-TO-PARA RATIO AND UPPER LIMIT ON THE D_2H^+ PARA-TO-ORTHO RATIO, VARYING THE COSMIC IONIZATION RATE, THE CORE AGE AND THE GRAIN RADIUS.

parameters			$\frac{o}{p} \text{ H}_2\text{D}^+$	$\frac{p}{o} \text{ D}_2\text{H}^+$
cosmic ionization rate (s^{-1})	age (years)	grain radius (μm)		
$3 \cdot 10^{-17}$	10^5	0.05	0.02	< 1.07
$3 \cdot 10^{-17}$	10^5	0.1	0.03	< 0.15
$3 \cdot 10^{-17}$	10^5	0.2	0.08	< 0.55
$3 \cdot 10^{-16}$	10^5	0.1	0.03	< 0.29
$3 \cdot 10^{-18}$	10^5	0.1	0.07	< 0.29
$3 \cdot 10^{-17}$	10^4	0.1	0.07	< 0.29
$3 \cdot 10^{-17}$	10^6	0.1	0.03	< 0.29
$3 \cdot 10^{-17}$	10^5	0.3	0.17	< 0.63
$3 \cdot 10^{-17}$	10^5	0.4	0.32	No solution
$3 \cdot 10^{-18}$	10^5	0.4	0.33	< 11.81
$3 \cdot 10^{-17}$	10^4	0.4	0.33	< 11.81

TABLE 3
CURRENT AND FUTURE FACILITIES FOR THE CHEMISTRY OF H_2D^+ AND D_2H^+ IN PRESTELLAR CORES,
PROTO-PLANETARY DISKS AND PROTOSTARS.

Name	Aperture	Platform	Available	H_2D^+		D_2H^+	
				$1_{1,0}-1_{1,1}$ (372.4 GHz)	$1_{0,1}-0_{0,0}$ (1.37 THz)	$1_{1,0}-1_{0,1}$ (691.7 GHz)	$1_{1,1}-0_{0,0}$ (1.48 THz)
CSO	10.4 m	Mauna Kea (USA)	Y	Y	N	Y	N
JCMT	15 m	Mauna Kea (USA)	Y	HARP B	N	Y	N
SOFIA	2.5 m	Airborne (747)	2007	N	Casimir GREAT (CONDOR)	Casimir	Casimir GREAT (CONDOR)
Herschel (HIFI)	3.5 m	Space (L2)	2007	N	N	Y	Y
ALMA	50 \times 12 m	Atacama (Chile)	2010	Y	N	Y	N
APEX	12 m	Atacama (Chile)	2005-2006	Y	CONDOR	Y	CONDOR